Fusion Engineering and Design 223 (2026) 115527

Contents lists available at ScienceDirect

Fusion Engineering and Design

journal homepage: www.elsevier.com/locate/fusengdes

Numerical analysis of 60° V-ribs for helium-cooled high heat flux loaded first wall, challenges and contributions

Ch. Klein *, F. Arbeiter, M Enke

INR KIT, Hermann von Helmholtz Platz 1 76344 Eggenstein-Leopoldshafen, Germany

ARTICLE INFO

Keywords:
Helium cooled first wall channels
Ribbed channels
CFD simulations

ABSTRACT

The HCPB (Helium Cooled Pebble Bed) blanket concept for EU DEMO fusion reactors employs high-pressure (8 MPa) helium gas as coolant for the plasma facing first wall (FW). Up-to-date estimates for the total maximum of heat flux go up to 0.73 MW/m². Higher short-term transient loads are possible. 60°-V-shaped ribs show high heat transfer and are thus the subject of the presented studies. Although Scale-Resolving Simulation (SRS) techniques such as LES (Large Eddy Simulation) are able to calculate heat transfer and pressure drop precisely, their application is limited to an individual ribs or a few mm channel segment due to the high required mesh count. Nevertheless, SRS techniques can be used to compare different ribs and to evaluate the performance of RANS (Reynolds-Averaged Navier-Stokes Simulations). Selected RANS models can be used to evaluate the development of secondary flow structures along the channel and compare complete channels with different rib configurations for thermohydraulic performance.

The objectives of the present paper are (i) to offer guidance on the range and limits of applicability of numerical methods when dealing with cooling flows in structured channels (sections 1–4) and (ii) to provide results on specific design features of surface structures (sections 5–7) that help designers in implementing thermal-hydraulic efficient yet fabrication friendly structured channels

Challenges like long entrance length and high material properties gradients are shown. Strategies for ribs height reduction with increasing heat transfer and reduction of pressure drop resulting in higher Cooling Performance Numbers (CPN) are found. Thermohydraulic performance of fabrication friendly ribs is calculated along the channel.

1. Numerical simulations of helium cooled first wall (FW) channels

The HCPB blanket concept for the EU DEMO fusion reactors employs high-pressure (8 MPa) helium gas as coolant for the plasma facing first wall. For the EU DEMO inboard blanket, the radiation heat flux on the FW is typically in the range of 0.15 – 0.27 MW/m². For the outboard blanket the radiation heat flux is typically in the range of 0.23 – 0.31 MW/m². The additional maximum of charged particle heat flux for the outboard blanket goes up to 0.42 MW/m². Significantly higher short-term transient loads are possible. In sum the total maximum of heat flux could go up to 0.73 MW/m² [1]. The definition of the peak values is ongoing and depends on the chosen shape of the first wall, the magnetic configuration and the assumptions about the fraction of the radiated power and the power decay lengths in the scrape-off layer (SOL) of the plasma. Efficient cooling has already been demonstrated in the past for heat flux densities of 1 MW/m² with helium channels equipped with transverse rectangular ribs on the plasma facing side. The simulations showed, that the structural material could be kept in the required temperature range with an acceptable pressure loss, and significantly less pumping power as required for a non-ribbed channel. 60°-V-shaped ribs show even 35 % higher heat transfer compared to transversal ribs, and are thus the subject of the presented studies [2].

Long term objectives of the qualification work for numerical simulations for the helium cooled First Wall channels of EU DEMO are to provide a consistent, fully validated and practically feasible (in terms of computing resources) numerical approach to provide simulations of complete rib enhanced FW channels/ full-size blanket components. Numerical simulations shall predict temperature fields within the FW Blanket components as a basis for thermomechanical requirements. Numerical simulations can also provide engineering correlations (for pressure drop, fluid outlet temperatures etc.) i.e. as input for the Balance

* Corresponding author.
E-mail address: Christine.Klein@kit.edu (Ch. Klein).

https://doi.org/10.1016/j.fusengdes.2025.115527
Received 3 February 2025; Received in revised form 30 August 2025; Accepted 12 November 2025
Available online 2 December 2025

of Plant (BoP) or codes. Another objective is to contribute to the design of thermo-hydraulic experiments to validate numerical codes and to contribute to the design of demonstrators or mock-ups.

The fluid dynamics problems of the FW with ribbed surfaces are characterized by a large spread of scales, which poses a serious challenge to numerical simulations:

- The channel length is in the order of 2 m. In a RSM simulation for a full FW channel without ribs, channel height of 12.5 mm at 60 g/s, the vortex pattern induced by the centrifugal forces of the inlet bend persisted for about 28 times the channel height, while development of the axial velocity profile was still seen at 36 times the channel height. Also, strong axial thermophysical property variations preclude the simplification to a segment with reduced length, when the component temperature field is desired.
- When ribs are employed ($e = 0.2 – 1.0$ mm height) eddies and flow features with a fraction of that size are produced and are effective for local heat transfer prediction and therefore need to be resolved.
- The high Reynolds numbers imply thin boundary layers (∼55 μm). Appropriate heat transfer models require grid resolution up to the wall, so that the first nodes must be placed typically within ∼2 μm or less distance from the wall.
- In the vicinity of the rib, where the streamlines are strongly curved, numerical requirements make it necessary to apply a fine resolution also in the coordinate perpendicular to the wall.

This large separation of scales that need to be resolved implies a very high mesh count, and in case of transient simulations like LES or Unsteady RANS (URANS) also very small-time steps (0.1 μs). As for now, it was therefore not possible to simulate a full FW channel (or relevant section) with SRS.

The present work therefore founds on two different approaches:

1. For the comparative study of detail features of the rib geometry, LES of channel segments comprising only a single rib element are used. Such simulations are in some respects representative for the far downstream region of the channels of interest. Secondary flow intensities are likely to be over-estimated over the ones that are effective in most parts of an FW channel with finite length.
2. For the study of evolution of flow features in streamwise direction, RANS models are used. Due to the Reynolds averaging, these models can't account for certain unsteady effects induced by the ribs, and are not credited to predict the correct heat transfer magnitude. However, the selected models are able to predict the major secondary flow features and therefore at least qualitatively reproduce the axial development of the flow field, also considering thermophysical properties variations.

2. Common pre-processing of FW channel simulations

2.1. Geometry

This section describes common aspects of all simulations discussed in this paper. The straight part of a FW cooling channel is ribbed at the plasma facing side. A channel section with one rib of the ribbed straight part of a FW Channel is illustrated in Fig. 1. The solid part of the channel has a height of $h = 22$ mm and a width of $w = 14.6$ mm. The flow cross section is quadratic with an edge length of $a = 12.5$ mm with rounded corners with $r = 1.5$ mm.

The cooling rib has a height of $e = 0.4$ up to 0.9 mm and designed as V-rib with a 60° angle of attack. Pitch to height ratio $p/e = 10$. Different rib arrangements are described in the respective sections

2.2. Boundary conditions and material properties

The channels were heated from the breeder side wall with a homogenous heat flux of $\dot{q}_{Br} = 80\text{kW/m}^2$ and from the plasma side wall with a homogenous heat flux of $\dot{q}_{Pl} = 1\text{MW/m}^2$.

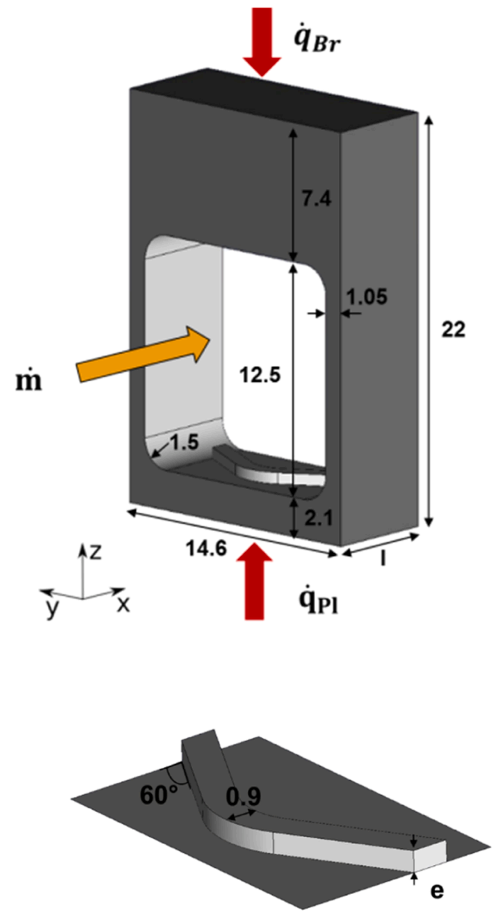

Fig. 1. Geometry of investigated channel (section), exemplary geometry of single V-shape rib.

1. For LES models with periodic boundary conditions, a mass flow rate $\dot{m}$ of 60 g/s is applied as periodic inlet/outlet condition and an operating pressure of $p = 8$ Mpa. For RANS models with elongated geometries, a velocity inlet with a bulk velocity of $u_0 = 62.9\ \frac{m}{s}$ and pressure outlet were used. $u_O = 62.9\text{m/s}$ is the bulk velocity, calculated with the formula $u_0 = \frac{\dot{m}}{\rho_0 A} = 62.9\ \frac{m}{s}$.

Helium enters with a temperature of $T = 623.15$ K. The Reynolds number is $Re = 156{,}000$.

For Eurofer steel material parameters are approximated for the expected temperature range by regression analysis from empirical data from Tavasolli [3] The specific heat capacity $c_p^E(T)$ and the thermal conductivity $\lambda^E(T)$ were defined a as a polynomial function of temperature in the form of eq. (1) with coefficients in Table 1.

$$\Phi\ (T) = A + B\cdot\frac{T}{K} + C\cdot\frac{T^2}{K^2} + D\cdot\frac{T^3}{K^3} + E\cdot\frac{T^4}{K^4}. \tag{1}$$

For helium the specific heat capacity $c_p^{He} = 5188$ J/(kg·K) was used, the thermal conductivity λ^{He} and the dynamic viscosity μ^{He} were defined

Table 1
Coefficients for Eurofer.

	A	B	C	D	E
$c_p^E(T)$	343.89	0.2356	0.003867	$-7.81\bullet10^{-6}$	$5.016\bullet10^{-9}$
$\lambda^E(T)$	54.44	−0.0723	$5.21\bullet10^{-5}$		

as polynomial functions of temperature. The coefficients in Table 2 were found by regression analysis from empirical data (at 8 MPa) from the National Institute of Standards and Technology [4]

2.2. Mesh details

ANSYS ICEM CFD software involving manually partitioning the geometry into logical hexahedral-friendly blocks was used to create a high-quality, structured, all-hexahedral mesh. For the LES quality conditions regarding the cell size $y^+ = \frac{y \cdot u_\tau \cdot \rho}{\mu}$ is calculated with the density ρ, the viscosity μ and the shear velocity u_τ. The shear velocity is $u_\tau = \sqrt{\frac{\tau_W}{\rho}}$. The wall τ_W shear stress is calculated with the friction coefficient above. The shear stress is

$$\tau_W = \frac{f_{0,P}}{8} \cdot \rho \cdot u_m^2 = 50.41 \frac{N}{m^2}$$

and the shear velocity $u_\tau = 2.8560 \frac{m}{s}$. With these values $y(y^+ = 1) = 1.8815 \cdot 10^{-6}$ m is calculated.

The boundary layer $y(y^+ = 70)$ adjacent to the walls was resolved by 20–30 nodes providing a wall-normal first spacing of $\Delta y^+ < 1$ and a growth factor in wall normal direction <1.2. The LES quality conditions of a non-dimensional maximum cell size recommended by Menter [5] ANSYS Best Practice: Scale-Resolving Simulations in ANSYS CFD in stream wise direction $\Delta x^+_{max} \leq 40$ and in span- and crosswise direction $\Delta y^+_{max} \approx \Delta z^+_{max} \leq 25$ were targeted for the big parts of all computational domains, but to reduce cell count due to limited computational capacity slightly exceeded in the middle of the channel, but the mesh was refined in flow regions close to the channel walls and the rib. Mesh studies for the LES simulations were performed, resulting in rib $e = 0.4$ mm: $19.8 \cdot 10^6$ hexahedral cells for the fluid domain and $6.3 \cdot 10^6$ hexahedral cells for the solid domain, together $23.1 \cdot 10^6$; rib $e = 0.6$ mm: $17.3 \cdot 10^6$ hexahedral cells for the fluid domain and $4.3 \cdot 10^6$ hexahedral cells for the solid domain, together $21.6 \cdot 10^6$ hexahedral cells, rib $e = 0.9$ mm $4.4 \cdot 10^6$ hexahedral cells for the fluid domain and $1.2 \cdot 10^6$ hexahedral cells for the solid domain, together $5.6 \cdot 10^6$ hexahedral cells.

3. Entrance length in a straight ribbed duct

In order to study the entrance length l_h of the rib-induced flow field, a long channel with 100 rib elements and a total length $l = 1$ m was studied. To isolate the effect of the ribs alone, the velocity profile at the entrance was taken from a developed flow in a straight channel. In a usual FW configuration, the straight part would be preceded by an inlet bend, that itself already induces strong secondary flows in the same sense as the ribs.

In order to capture the developing hydraulic boundary layer and secondary flows, a simulation with a Reynolds stress equation model was performed with a rib height e of 0.9 mm and a pitch to height ratio $p/e = 10$. The individual components of the Reynolds stress tensor are directly computed in order not to rely on the eddy-viscosity hypothesis and capture also effects of anisotropic turbulence.

The results in terms of the velocity in x direction u_x normalized with the reference velocity $u_0 = 62.9 \frac{m}{s}$ can be seen along the channel in Fig. 2. The ribs induce two counter-rotating vortices with velocity direction towards the ribs in the middle. The action of these secondary flows leads to the development of two local maxima of the axial velocity.

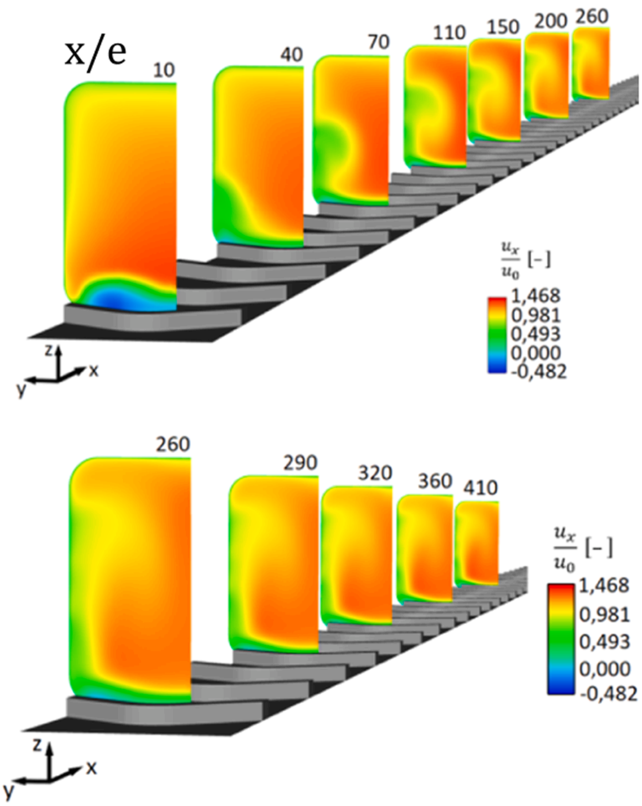

Fig. 2. Velocity fields for straight v-ribbed ($e = 0.9$ mm) part of FW channel in flow direction. Sections are labelled with normalized axial position x/e.

A low-speed plume surges upwards near the side walls and enters into the core flow field. It takes more than $l_h \sim 38 d_h$ (approximately half of channel) till the secondary flow is developed, resulting in high mesh count. A similar length is found for the development of the temperature fields till they are roughly constant.

Table 2
Coefficients for helium properties.

	A	B	C	D	E
$\mu^{He}(T)$	4.97495 $\bullet 10^{-6}$	5.83121$\bullet 10^{-8}$	3.03782 $\bullet 10^{-11}$	1.84653 $\bullet 10^{-14}$	5.13833 $\bullet 10^{-18}$
$\lambda^{He}(T)$	0.0393442	2.64539 $\bullet 10^{-}$	2.64539 $\bullet 10^{-7}$	4.63622 $\bullet 10^{-14}$	

4. Magnitude of spatial material properties gradients

Another challenge for numerical simulation arises from the high heat flux. The high flux from the plasma side wall $\dot{q}_{Pl} = 1 MW/m^2$ results in high temperatures and material properties gradients. A section of a flat non-ribbed FW channel is calculated with Menter's Shear Stress Transport turbulence model (SST), combining the k-omega- and k-epsilon turbulence model. Periodic boundary conditions had been applied. In Fig. 3 the contours of the density of helium are shown in a cross section perpendicular to the flow direction x. Due to the temperature differences the density at the plasma facing wall is 54 % lower directly at the wall as

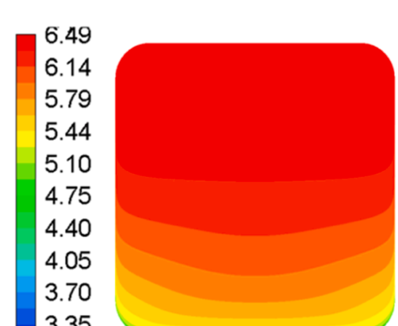

Fig. 3. Density of helium in cross section perpendicular to the flow direction x (1 MW/m: ²).

Table 3
Comparison RSM and LES for different rib heights.

	$e = 0.4$ mm		$e = 0.6$ mm		$e = 0.9$ mm	
	RSM	LES	RSM	LES	RSM	LES
$\overline{Nu}_p$	2.3	2.58	2.33	2.45	1.86	2.35
$/Nu_n$	− 10.8%		− 9.1%		− 24.7%	
f_D/f_0	3.76	2.95	4.45	4.34	5.07	5.24
	+ 27.4%		+ 2.46%		− 3.2%	
CPN	1.02	1.3	0.98	1.07	0.72	0.96
	− 21.5%		− 10.9%		− 25%	

compared to the core flow.

The same effects show up with other material properties of helium. There is up to 33 % decrease of the thermal conductivity and up to 30 % increase of the dynamic viscosity of the helium at the plasma side wall. The increase of the dynamic viscosity results in a decreased local Reynolds number near the wall, and also the decreased density effects a reduced convective and turbulent transport in the wall region.

For the material Eurofer steel due to the heat flux there is a 10 % decrease of thermal conductivity and 58 % decrease of specific heat capacity in the experienced temperature field compared to the core flow.

Under such conditions, significant errors show up, if constant properties were used. On the other hand, temperature dependent properties can be a source of numeric instabilities and increase the computational effort.

5. Effect of rib heights calculated with RSM and LES on a periodic segment

Simulations to assess the effect of the rib height of v-ribs were done comparatively with LES and RSM, both using periodic boundary conditions on a channel segment with a single rib. The results for the normalized friction factor f_D/f_0 and over the bottom plate averaged and normalized Nusselt number $\overline{Nu}_P/Nu_0$ on the plasma facing channel side are compared for three different rib heights (0.4, 0.6 and 0.9 mm). The following normalization scales were used: the Nusselt number $Nu_0 = 243$ is calculated by the Gnielinski correlation [6] and the Petukhov [7] Darcy friction factor $f_0 = 0.016$.

Additionally, the cooling performance number $CPN = \frac{37.07 \cdot Nu^{1.18}}{Re \cdot f^{1/3}}$ was calculated. A more detailed description of CPN (cooling performance number) is given in a paper of Ruck et al. [8]. The CPN (cooling performance number) is based on the thermal performance evaluation concept by Fan et al. [9] and relates the gains in heat transfer with the costs in friction factor. The results can be shown in Table 3.

RSM gave an under-estimation of the heat transfer vs. the LES in all cases. The under-estimation of heat transfer was up to 27 %. A good match of the values for the friction factor for the higher ribs 0.6 and 0.9 (here max difference 3.2 %), less for the smaller rib of 0.4 mm was obtained.

The LES Simulation of the different rib heights in Table 3 show

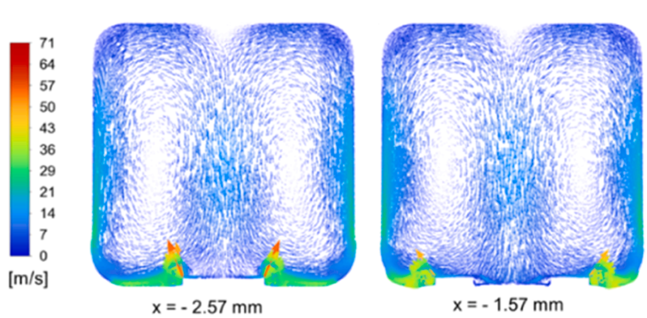

Fig. 4. Rib $e = 4$ mm mean secondary velocity field, -x view, different x pos., volume averaged secondary velocity 8.13 m/s.

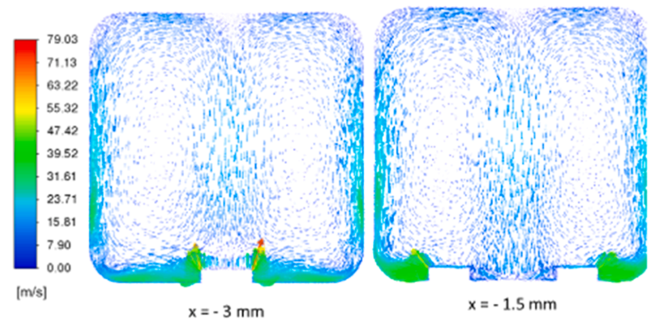

Fig. 5. Rib $e = 6$ mm mean secondary velocity field, -x view, different x pos., volume averaged secondary velocity 9.52 m/s.

promising effects on the Nusselt number, friction factor and the CPN values. The friction factor is increasing with the rib height, but not the Nusselt number. The Nusselt number is even higher for smaller rib heights. The reasons for similar heat transfer are the roughly same secondary flow values for different rib heights. These vortices (filling the whole channel cross section), shown in Fig. 4 till Fig. 6, for the LES simulations, are significantly contributing to the high heat transfer. The secondary flow velocity is calculated Fig. 5

$$v_s = \sqrt{u_y^2 + u_z^2}$$

and volume averaged secondary flow:

$$v_{MS} = \frac{1}{V} \int_V \sqrt{u_y^2 + u_z^2} dV.$$

In Table 4 average secondary mean velocity v_{MS} for LES and RSM for different rib heights are compared.

However, it has to be taken onto account that these simulations are done with periodic boundary condition. The values can be interpreted as thermal and hydraulic developed flow and over-estimate the secondary flow velocities vs. the ones that are effective in a real channel of finite length.

6. Effect of rib height for thermal and hydraulic developed flow

The findings reported in Section 5 on the impact of rib height on heat transfer and pressure drop opens up the opportunity to decrease the rib height in case of already developed secondary flow, which means in the downstream part of a ribbed FW channel behind the bend, as shown in 7. The idea is to use higher ribs in the upstream part to induce strong secondary flows and then use smaller ribs in the downstream part of a FW channel to maintain the secondary flow intensity, but save friction resistance.

This approach was verified by two comparative simulations of two 900 mm long channels: Channel “A” was equipped with ribs with the height $e_A = 0.9$ mm (pitch to height ratio $p_A/e_A = 10$) along its full length, as presented in Section 3 above. Channel “B” is identical to channel “A” for the first 504 mm after the entrance. However, in its downstream section (> 504 mm up to 900 mm) the channel is equipped with smaller ribs, height $e_B = 0.4$ mm (pitch to height ratio $p_B/e_B = 10$). Technically, channel “B” was simulated by imposing the profiles of simulated quantities sampled from channel “A” at x_A=504 mm to the inlet surface of a shorter simulation domain, which represented the downstream part of channel “B” with the extent $0 \leq x_B \leq 396$ mm. The topology of both channels respectively simulation domains is sketched in Fig. 7.

A RSM is used to compare the performance of these two channel models. The pressure along the flow direction x can be seen in Fig. 8.

The red line in Fig. 8 shows the pressure along the flow direction for channel “A” with the 0.9 mm ribs. The thick black line shows the

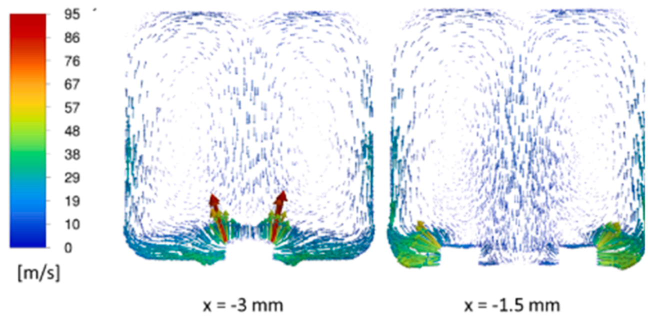

Fig. 6. Rib $e = 9$ mm mean secondary velocity field, -x view, different x pos., volume averaged secondary velocity 9.46 m/s.

Table 4
Comparison average secondary mean velocity $\boldsymbol{v_{MS}}$ for LES and RSM for different rib heights.

v_{MS}	$e = 0.4$ mm	$e = 0.6$ mm	$e = 0.9$ mm
LES	8.13 m/s	9.52 m/s	9.46 m/s
RSM	5.37 m/s	6.79 m/s	5.5 m/s

pressure in the downstream part of channel B. In the downstream section, channel "B" with the 0.4 mm ribs shows ~45 % lower pressure gradient compared to channel A. This means for the complete channel B a ~22.5 % lower pressure drops.

In Fig. 9 the normalized Nusselt number on the plasma facing channel side along the flow direction for the complete channel A (red dots) with the 0.9 mm ribs and complete channel B (red dots) with the 0.4 mm ribs is visualized.

The normalized Nusselt numbers values stabilize in channel A ougly at $x = 500$ mm (x/dh = 38). While the normalized Nusselt numbers in the downstream part of channel A reaches values between 1.8 and 1.9, values above 2.3 are reached for channel B. This values show good agreement with the values in Table 3 (2.3 and 1.89) caculated for single 0.4 and 0.9 mm ribs with periodic boundary conditions with the RSM. It is concluded that the ribs of channel B, which have a lower profile than those of channel A, but are more densely arranged (more ribs per surface area of the channel) can effect a better heat transfer than the higher profile ribs of channel A. We have for the downstream part of channel B (with ribs $e = 0.4$ mm) even higher Nusselt numbers and at the same time lower pressure drop.

7. Thermal-Hydraulic performance of chamfered rib variants along the FW channel

In a Reynolds stress (RS) turbulence model the individual components of the Reynolds stress tensor are directly computed, significantly better accuracy for the flow fields can be achieved. A RS model is used for a comparative study of two different 60° V-rib types "AV2stc" and "AV2s", as shown in Fig. 10: They both have "fabrication friendly" chamfers (2 mm radius) at the upstream and downstream edge of the rib. The version AV2**stc** (**s**hortened rib, only 7 mm wide, due to the increase of the channel corner radius with a rounded chamfer $R = 1$ mm, **t**ips **c**hamfered) has additional chamfers at the rib tips, while the AV2s version has 90° rectangular cornered tips. It was the objective to assess the impact of this fabrication-relevant detail on the thermal-hydraulic performance. The simulated channels were 500 mm long (roughly the expected hydraulic entrance length), the heat load on the plasma side was 750 kW/m² and the mass flow of helium was 60 g/s. Deviant to the geometries presented above, those channes have a height of 15 mm and corner radii of 4 mm.

The Nusselt number in x direction on the straight channel part on the plasma facing side is visualized in Fig. 11a) for the AV2stc ribs and in Fig. 11b) for the AV2s ribs. The average Nusselt number in the straight channel part for the AV2stc ribs is $\overline{\mathrm{Nu}}_{\mathbf{Pl}} = 361(\overline{\mathrm{Nu}}_{\mathrm{Pl}}/\mathrm{Nu}_0 = 1.39)$ and as such 15 % smaller than the average Nusselt number for the AV2s ribs, which is $\overline{\mathrm{Nu}}_{\mathbf{Pl}} = 427$ $(\overline{\mathrm{Nu}}_{\mathrm{Pl}}/\mathrm{Nu}_0 = 1.64)$. Accordingly, the effective rib length reduction by the tip chamfering is seen to have a significant reducing effect on heat transfer performance.

The average pressure gradient in the straight channel part is 17,248 Pa/m $\left(\frac{f_D}{f_0} = 1.89\right)$ for the AV2stc ribs and 20,691 Pa/m $(\frac{f_D}{f_0} = 2.27)$ for the AV2s ribs. As to be expected, the reduced blocking by the tip chamfer reduces the pressure drop.

8. Summary,Conclusions and outlook

Complementary use of LES and RANS models was used to address research questions associated with optimizing the rib pattern for the helium cooled FW that can allow efficient operation at heat flux densities up to 1 MW/m².

It was found by a RSM on a long domain that the hydraulic entrance length of a v-ribbed channel was about 38 times the hydraulic diameter. This precludes the reduction of FW engineering related problems to the simulation short segments. Further, it was found that the high temperature gradients in helium FW flows exposed to 1 MW/m² heat fluxes induce variations of 30 – 50 % of the thermophysical properties, thus counter-indicating the use of constant properties models.

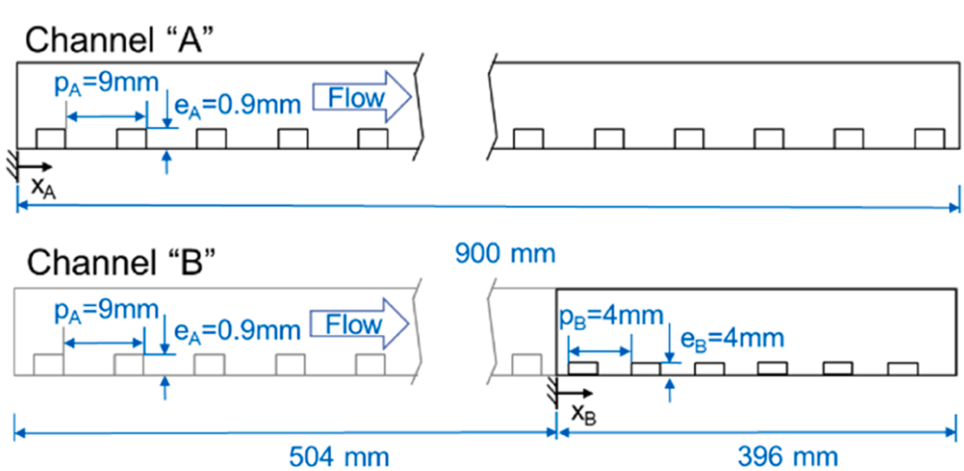

Fig. 7. Topology, measures and coordinate definitions of channel A (constant rib height) and channel B (variated rib height).

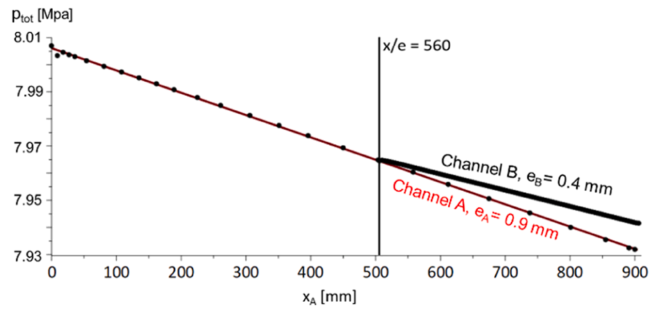

Fig. 8. Pressure along the flow direction x for channel A (red) and B (black).

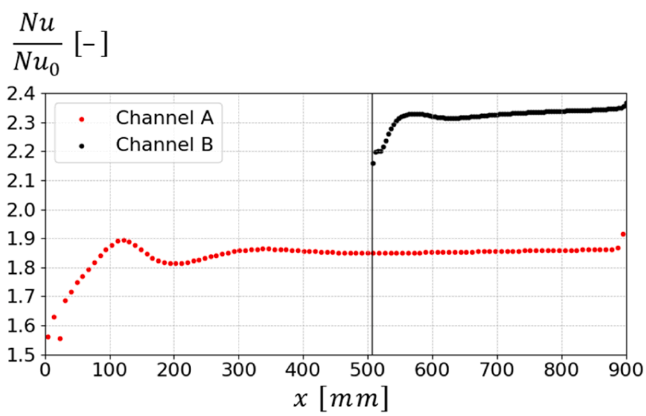

Fig. 9. Normalized Nusselt numbers Nu/Nu_0 on the plasma facing channel side along the flow direction x for channel A (red dots) and channel B (black dots).

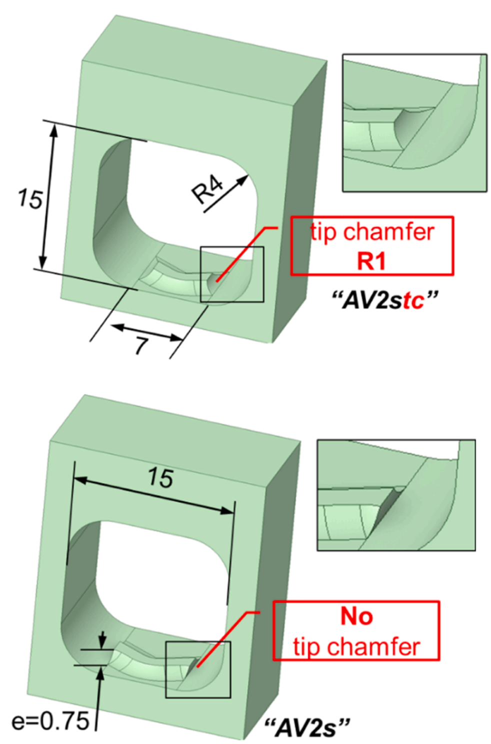

Fig. 10. Geometry of AV2stc rib with $r = 1$ mm tip chamfer and AV2s rib with cornered rib tips.

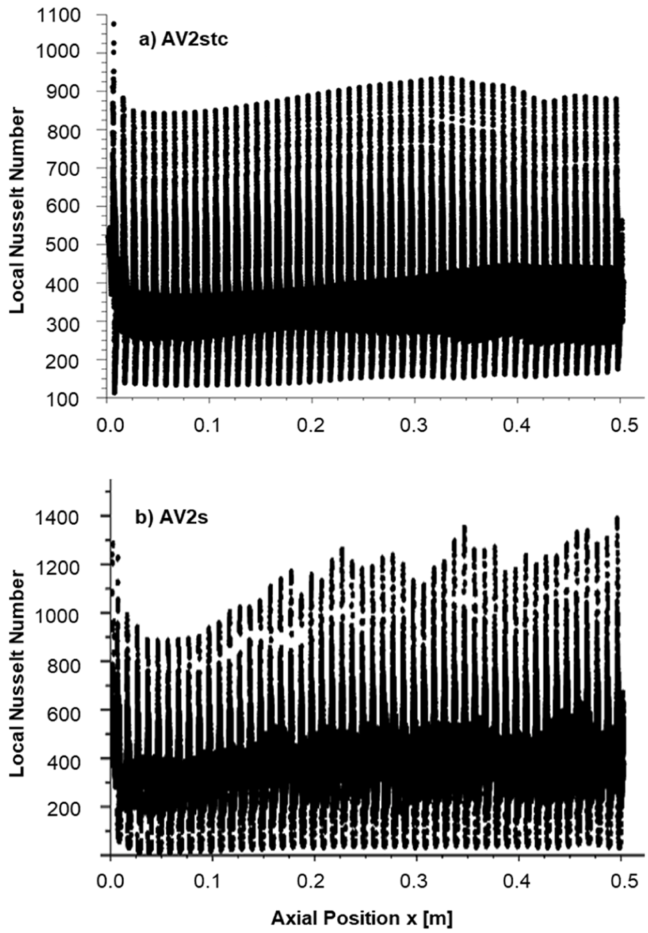

Fig. 11. Nusselt number Nu on the plasma facing channel side along the flow direction x for the AV2stc ribs a) AV2stc ribs, Below, b) AV2s ribs.

A comparative study applying both LES (regarded as reference) and RSM to short channel sections with periodic boundary conditions revealed significant differences between the two modelling approaches, with 25 % lower heat transfer predicted by RSM. This clearly shows a deficiency of RSM to model the absolute level of heat transfer in the studied rib geometries. The LES predictions of the different ribs models shall serve as target data to tunne the generalized k-omega (GEKO) turbulence model by adjusting its calibration parameters to be able to calculate complete rib enhanced FW channels/ full-size blanket components with higher precision as the RSM especially heat transfer and pressure drop.

The study of rib height variations in those models gave a first indication that v-rib height with a height of 0.4 mm would be expected to yield a superior cooling performance (better cooling per pumping power) in comparison to the high profile ribs with 0.9 mm, investigated earlier. This finding was confirmed in a RSM study on long channels, where the rib height was variated over the axial length.

Comparative RSM studies were also applied to investigate the impact of a geometry detail such as a tip chamfer of the v-ribs. It was found that such a detail can have a significant impact (~ 20 %) both on pressure drop and heat transfer. Both"fabrication-friendly" rib types AV2stc and AV2s show smaller Nusselt numbers (- 40 %, −30 %) than the 0.6 mm high rectangular rib in chapter 5.

This comparative evaluation of the rib heights and shapes shall support decisions for choosing heat transfer-enhanced wall structures for Demo including simulation stability, heat transfer and manufacturing.

CRediT authorship contribution statement

Ch. Klein: Writing – review & editing, Writing – original draft, Supervision, Methodology, Investigation, Conceptualization. **F. Arbeiter:** Supervision. **M Enke:** Investigation.

Declaration of competing interest

The authors declare that they have no known competing financial interests or personal relationships that could have appeared to influence the work reported in this paper.

Acknowledgments

This work has been carried out within the framework of the EUROfusion Consortium, funded by the European Union via the Euratom Research and Training Programme (Grant Agreement No 101052200 — EUROfusion). Views and opinions expressed are however those of the author(s) only and do not necessarily reflect those of the European Union or the European Commission. Neither the European Union nor the European Commission can be held responsible for them."

Data availability

Data will be made available on request.

References

[1] F. Maviglia, EFDA_D_2P985Q v1.8 - DEMO-JUS-1-CD1-DEMO PFC Surface Heat Load Specifications, 2020. https://idm.euro-fusion.org/default.aspx?uid=2P985Q.
[2] F. Arbeiter, Y. Chen, B. Ghidersa, C. Klein, H. Neuberger, S. Ruck, G. Schlindwein, F. Schwab, A. Weth, Options for a high heat flux enabled helium cooled first wall for DEMO, Fusion Eng. Des. 119 (2017) 22–28.
[3] F. Tavassoli, Fusion Demo Interim Structural Design Criteria (DISDC) Appendix A Material Design Limit Data, TW4-TTMS-005-D01, CEA, 2004.
[4] National Institute of Standards and Technology, „NIST Standard Reference Database Number 69.,", 2018 [Online].
[5] F. Menter, Best Practice: Scale-Resolving Simulations in ANSYS CFD, ANSYS, 2012.
[6] V. Gnielinski, New equations for heat and mass transfer in turbulent pipe and channel flow,", Int. J. Chem. (1976) 359–368. S.
[7] B. Petukhov, Heat transfer and friction in turbulent pipe flow with variable physical properties, Adv. Heat Transfer., Bde 6 (1970) 503–564, https://doi.org/10.1016/S0065-2717(08)70153-9. S.
[8] S. Ruck, F. Arbeiter, Detached eddy simulation of turbulent flow and heat transfer in cooling channels roughened by variously shaped ribs on one wall, Int J Heat Mass Transf. 118 (2018) 388–401. Bd.S.
[9] F. Fan, A performance evaluation plot of enhanced heat transfer techniques oriented for energy-saving, Int. J. Heat Mass Transf. (2009) 33–44.